Electronic Supplementary Material (ESI) for RSC Advances.
This journal is © The Royal Society of Chemistry 2016

Spectroscopic Tracking of Mechanochemical Reactivity and Modification of a Hydrothermal Char

Michael T, Timko,[1*] Alex R. Maag,[1] Juan Mauricio Venegas[1], Brendan McKeogh,[1] Zhengyang Yang,[1] Geoffrey A. Tompsett[1], Simón Escapa,[1] Joseph Toto[1], Erin Heckley[1], and Frederick T. Greenaway[2]

[1]*Department of Chemical Engineering, Worcester Polytechnic Institute, 100 Institute Rd, Worcester, MA 01609.*

[2]*Carlson School of Chemistry and Biochemistry, Clark University, 950 Main St, Worcester, MA 01610*

Supporting Information.

The Supporting Information contains details on: 1) HTC synthesis, 2) XRD, 3) fitted Raman spectra, 4) an alternative Raman fitting procedure, 5) ESR line shape analysis, 6) ESR spectra obtained under vacuum conditions to exclude the effect of adsorbed oxygen on the HTC signal, 7) supplemental SEM micrographs of native and milled char, 8) data on HTC bond energies.

1. HTC Synthesis

Figure SI-1 contains photographs of the HTC synthesis process, including: the PTFE-lined reactor; HTC filtration and filtrate; recovered HTC; and dried HTC.

Figure SI-1. Photographs of HTC synthesis, filtration, recovery, and dried product.

* Author to whom correspondence should be addressed. E-mail: mttimko@wpi.edu

2. Detailed DRIFTS C-H Fitting

The main text briefly summarizes results obtained from fitting the C-H stretch region of HTC DRIFTS spectra. Figure SI-2 provides greater detail, showing in parts (a)-(e) the baseline-

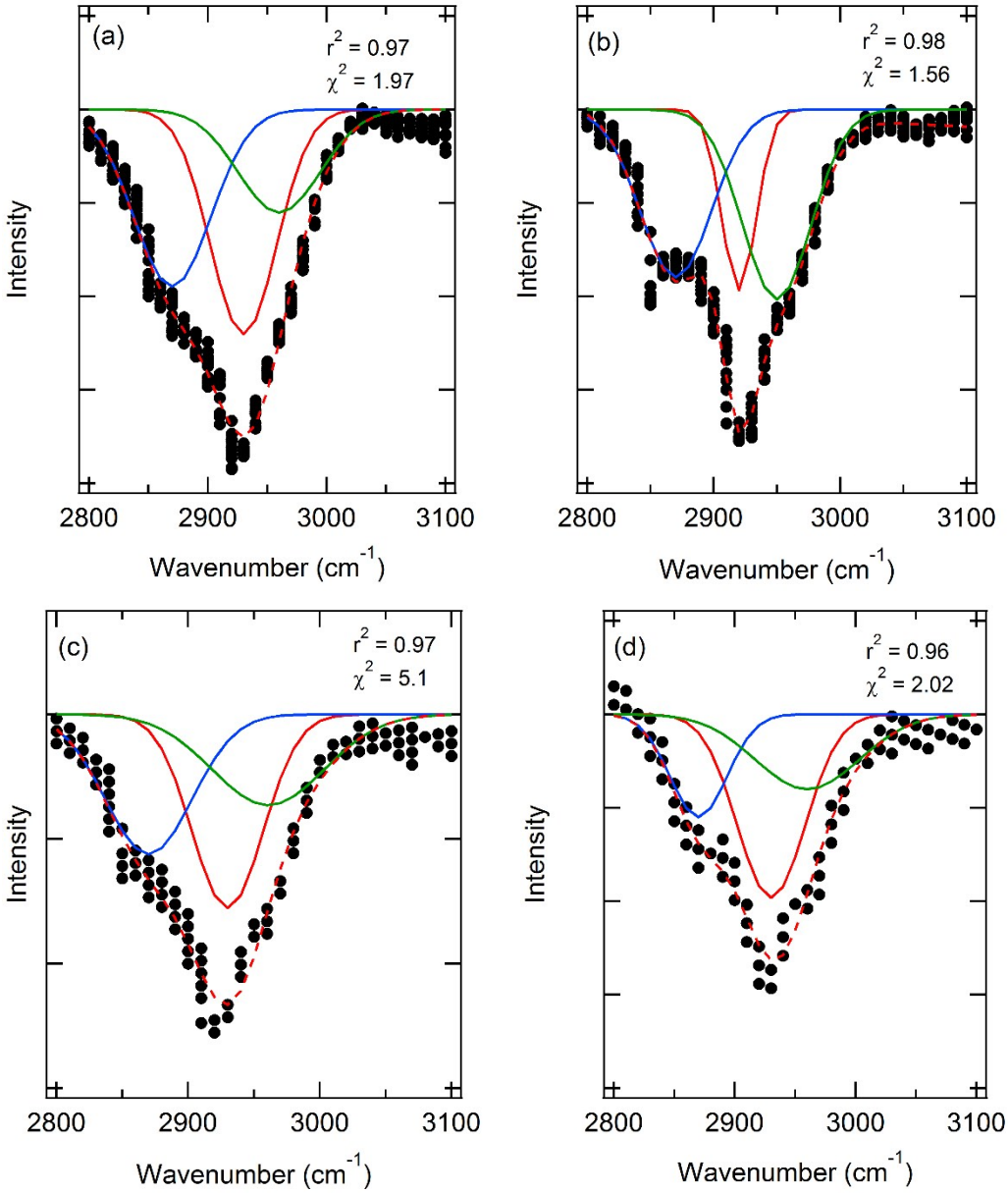

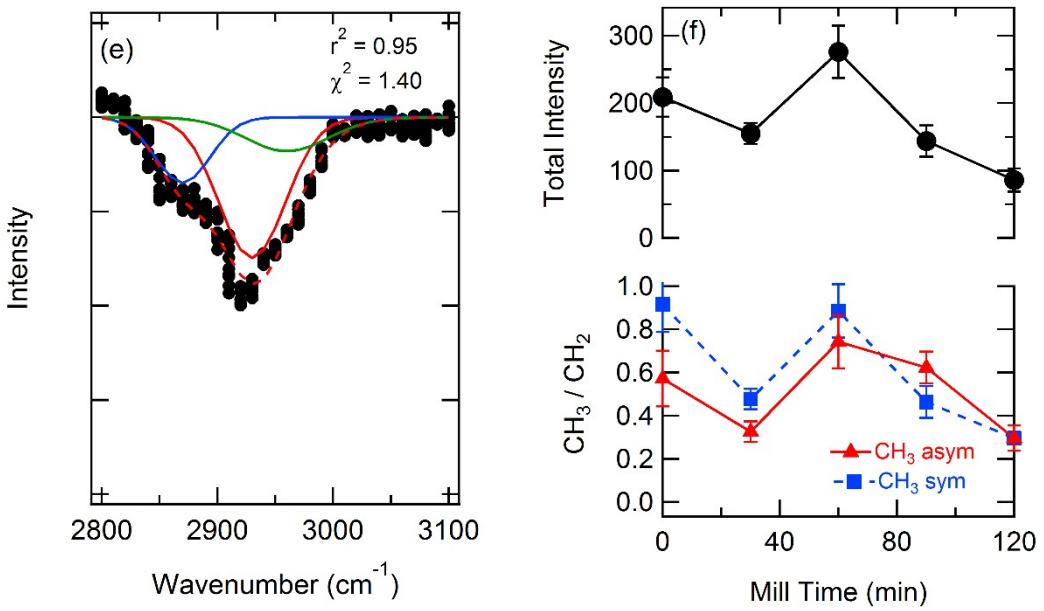

Figure SI-2. Fitting details of the C-H stretch region of the HTC DRIFTS spectra: a) synthesized HTC; b) HTC milled for 30 min; c) 60 min; d) 90 min; e) 120 min; f) summed intensity of the 2870 (CH_3 sym), 2930 (CH_2 asym), and 2960 (CH_3 asym) cm^{-1} peaks, CH_3 (asym) to CH_2 (asym) ratio, and CH_3 (sym) to CH_2 (sym) ratios plotted as functions of mill time.

corrected fits for DRIFTS spectra obtained for synthesized HTC and HTC milled for 30, 60, 90, and 120 min. In all cases, the spectra were fit with 3 Gaussians centered at 2870, 2930, and 2960 cm^{-1}. We select these positions based on comparison of the HTC DRIFTS spectra with the IR spectra for asphaltene, soot, and carbon black reported by Russo et al.[1] In comparison, our spectra resemble most closely those of asphaltene, largely on the basis of the minor contribution of the aromatic C-H stretch to both the HTC and asphaltene spectra. Accordingly, we used the the asphaltene assignments of Russo et al.[1] as a starting point for HTC fitting.

Because of differences in the IR methods, the HTC DRIFTS spectra shown in Figure SI-2 have lower resolution and a less well-behaved baseline compared to the Russo et al. [1] IR spectra, thus requiring some modifications to the fitting procedure. Hence, while Russo et al. [1] use 6

Gaussians to fit the C-H stretch region, we opted to use only 3 to describe the symmetric CH_3 stretch at 2870 cm^{-1}, the asymmetric CH_2 stretch at 2930 cm^{-1}, and the asymmetric CH_3 stretch at 2960 cm^{-1}. The symmetric CH_2 stretch that Russo et al.[1] observed for asphaltene at 2848 cm^{-1}, the aromatic C-H stretch at 3041 cm^{-1}, and the C-H stretch observed at 2896 cm^{-1} were not included in the HTC fits. Of these, the symmetric CH_2 stretch and the aromatic C-H stretch were likely obscured by the baseline, the latter primarily by the pronounced O-H stretch present in HTC but completely absent in asphaltene. The absence of the C-H band, which lies in the middle of the C-H region and is therefore not as prone to be obscured by baseline correction as the symmetric CH_2 stretch or the aromatic C-H stretch, suggests that this carbon form is not a major species in the HTC. Accordingly, adding the C-H stretch to the fit did not improve the goodness of fit. Additionally, we found that the asymmetric CH_3 stretch was better described by a Gaussian centered at 2960 cm^{-1} instead of the 2853 cm^{-1} recommended by Russo et al.[1] for asphaltene. Instead, we use the position that Russo et al.[1] recommend for a standard aromatic species; given that the CH_3 assignments suggested by Russo et al.[1] vary by approximately 14 cm^{-1} (2962 cm^{-1} for an aromatic species to 2948 cm^{-1} for soot), the 7 cm^{-1} shift used here is not unreasonable.

The 3-peak fit to the DRIFTS spectra are shown in Figure SI-2 in direct comparison with the raw data. In all cases, we fixed the peak positions (at 2870, 2930, and 2960 cm^{-1}, respectively) and regressed only the peak heights and widths. Regression parameters (r^2 and χ^2) are shown in each spectrum. Overall, r^2 is always greater than 0.95 and χ^2 less than 5.1, suggesting that reasonably good fits were obtained. We note that superior fits could be obtained by including the peak positions in the regression analysis, but decided that a consistent physical interpretation was more important than residual minimization.

Figure SI-2f contains plots of various DRIFTS-extracted data as functions of milling time: 1) the total sum of the peak areas of the 3 peaks, 2) the area ratio of asymmetric CH_3 peak to the asymmetric CH_2 peak, 3) the area ratio of the symmetric CH_3 peak to the asymmetric CH_2 peak. Error bars are estimated based on duplicate data and goodness of fit parameters. The trends for all three C-H stretches are similar, all passing through a maximum at 60 min of milling. For subsequent times (90 and 120 min), all 3 decrease to values similar to or less than their originals. From this, we conclude that CH species are lost during milling (hence the decrease in the total integrated area of the C-H stretch) and that preferentially CH_2 species are lost compared to CH_3. The preferential disappearance of the CH_2 species compared to CH_3 may suggest that CH_2 is initially present largely as a bridging carbon between adjacent aromatic rings, resulting in a weak C-C bond that can be readily cleaved.[2] In any event, Figure SI-2 provides further evidence of mechanochemical modification of the HTC that further augments the Raman and ATR-IR data presented in the main text.

3. XRD

The synthesized HTC and milled HTC were analyzed using XRD. Figure SI-2 contains the results. In all cases, XRD patterns of the carbon catalysts exhibited two broad peaks at $2\theta = 24$ and 42° (Figure SI-2). Babu and Seehra[3] attributed these diffraction peaks to the (0 0 2) and (1 0 0) or (1 0 1) planes of graphite crystallites, respectively. The XRD pattern did not change noticeably in any of the samples, indicating that ball milling resulted in no change of the long-range crystallinity.

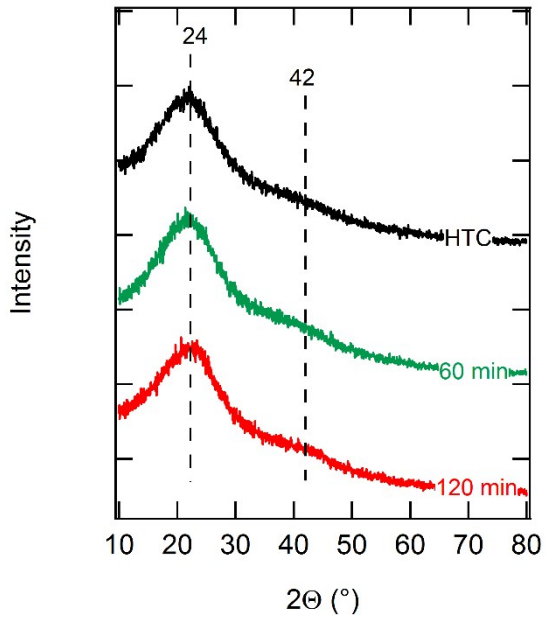

Figure SI-3. X-ray diffraction patterns of the as-prepared HTC and after balling for 60 and 120 minutes.

4. Fitted Raman Spectra: The G, D1, D2, D3, and D4 Fitting Procedure

In the text, we provided representative Raman spectra obtained for the synthesized HTC and HTC that had been milled for 200 min. Figure SI-4 reproduces these spectra and provides spectra obtained for HTC samples milled for 30, 60, 90, 120, and 300 min. In all cases, the residual is less than 0.1% in the range from 1100 to 1700 cm^{-1}. Only in the "wings" (i.e. less than 1100 cm^{-1} and greater than 1700 cm^{-1}) does the residual become larger than 1%.

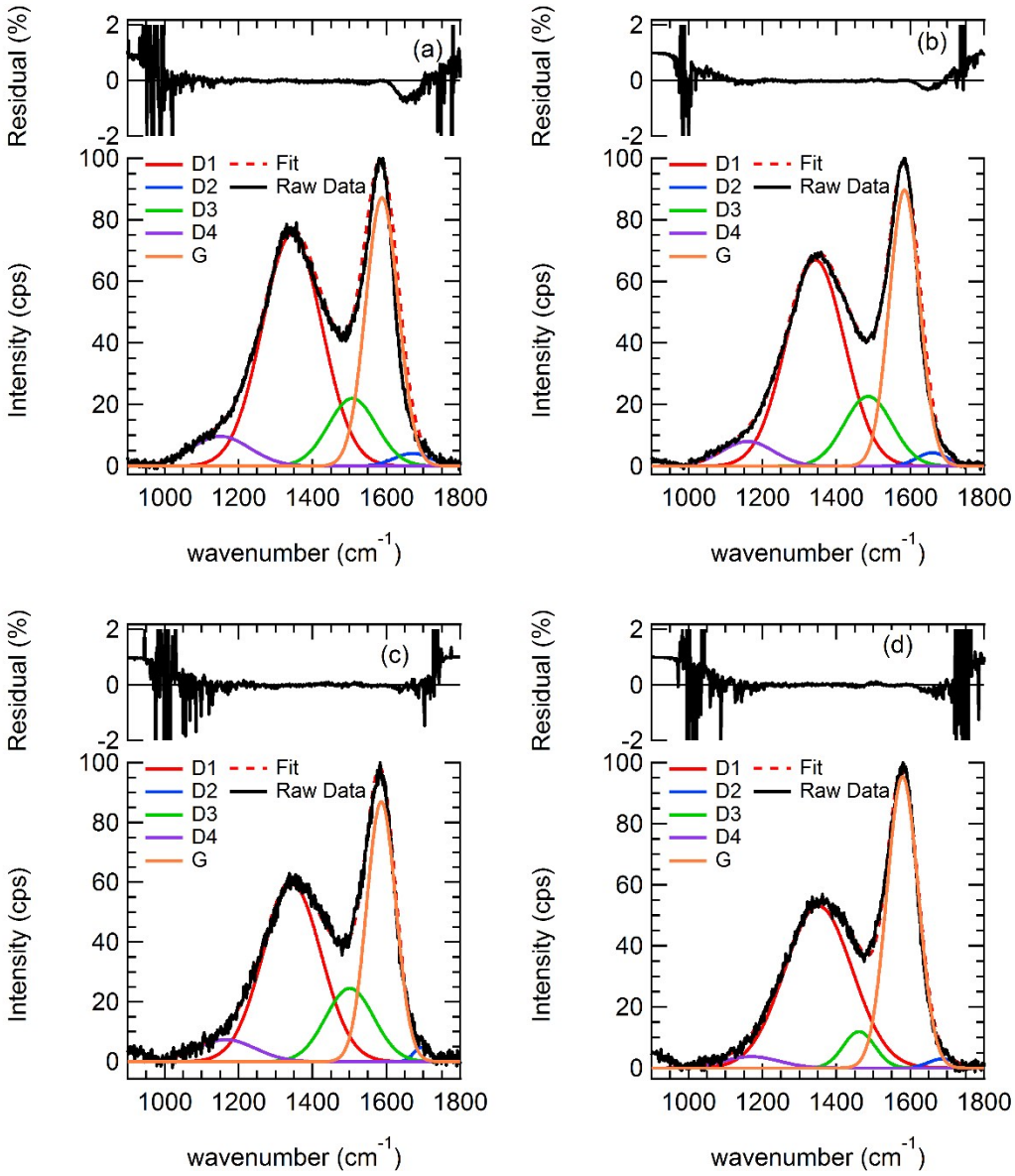
(a)
(b)
(c)
(d)
Residual (%)
Intensity (cps)
wavenumber (cm-1)
D1
D2
D3
D4
G
Fit
Raw Data

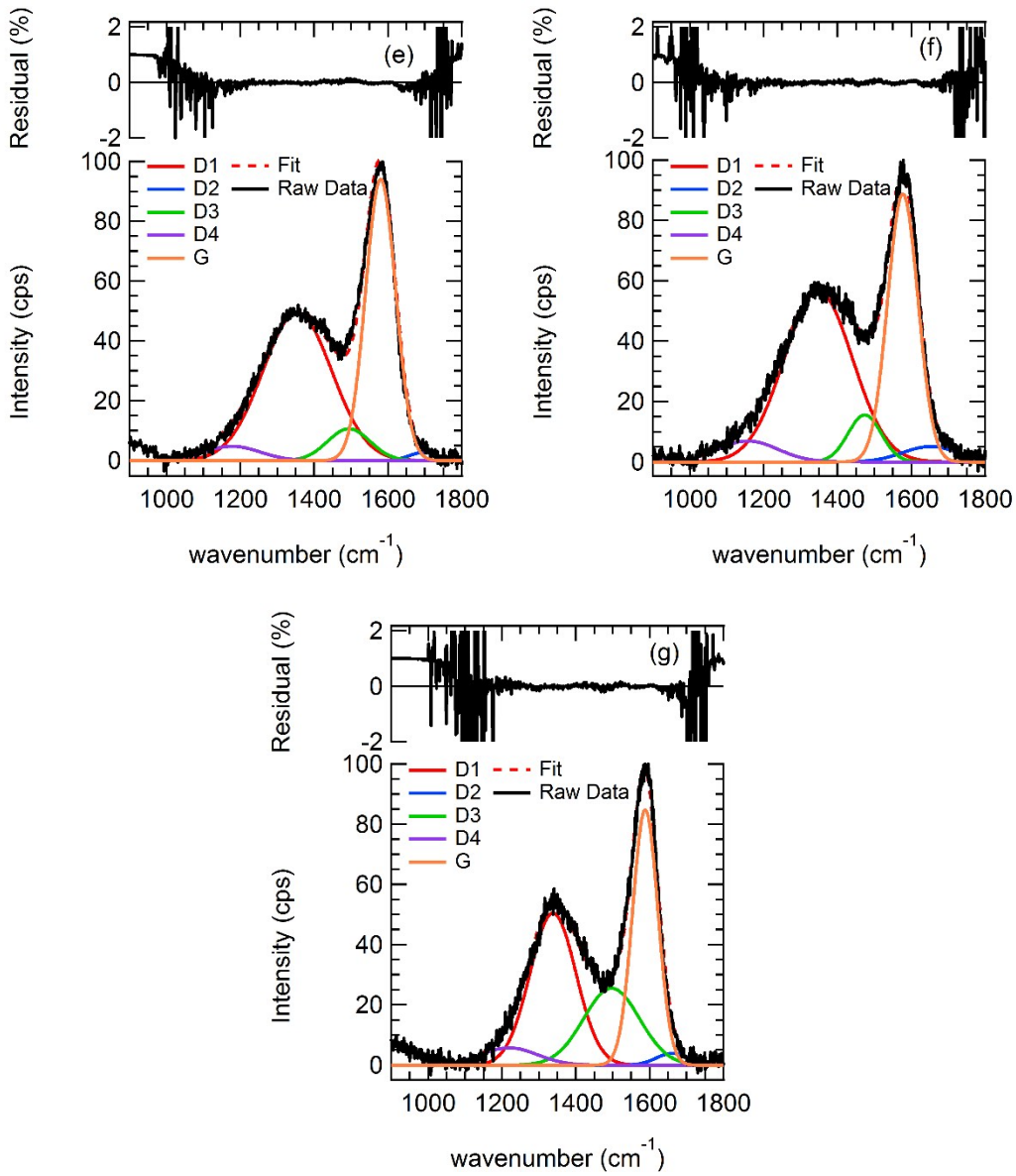

Figure SI-4. Representative Raman spectra and fits [4] for: a) synthesized HTC, b) 30 min milling, c) 60 min milling, d) 90 min milling, e) 120 min milling, f) 200 min milling, g) 300 min milling.

5. Alternative Raman Fitting Procedure

In the main text, we presented the Raman spectra fitting procedure articulated by Sadezky et al.[4] based on previous experiments on various carbon materials.[5, 6] More recently, the Sadezky et al.[4] assignments have been extended to many different carbon types.[7, 8] Based on its high level of

literature acceptance, we consider the Sadezky et al.[4] assignment scheme to be the most robust available for disordered carbon materials. In addition, we examined an alternative scheme suggested by Li et al.[9] for brown coals, and only partially applied to HTC.[10] We summarize these assignments in Table SI-1. Although the Li et al.[9] assignments have not been extended to carbons other than brown coal; their assignments were based on a careful review of the relevant literature and supported by additional spectroscopic characterization of model compounds. Moreover, the Li et al.[9] assignments provide a much more detailed molecular perspective than the Sadezky et al.[4] scheme. These combined considerations motivated our application of the Table SI-1 assignments to the HTC spectra. As we summarize here, the conclusions that we draw based on the Li et al.[9] assignments are broadly consistent with those described in the text from the Sadezky et al.[4] approach. However, likely due to the larger number of fitted peaks (9 compared to 5) in the Li et al.[9] scheme it results in trends with greater uncertainties than obtained using the Sadezky et al.[4] method. Hence, we provide the results of the Sadezky et al.[4] assignments in the main text and the Li et al.[9] assignments in the Supporting Information.

Table SI-1: Raman band assignments for HTC materials (adapted from Li et al.[9]).

Band Label	Position (cm^{-1})	Assignment	Structure
G_L (R)	1700	Carbonyl group	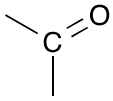
G	1590	Aromatic ring quadrant breathing, alkene C=C	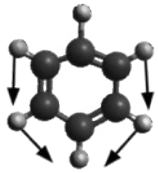
G_R	1540	Aromatic chains with <6 rings	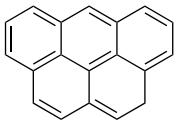
V_L	1465	Methylene & methyl groups, amorphous carbon structures	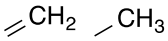
V_R	1380	Methyl group, amorphous carbon structures	
D	1300	Aromatic chains with 6 or more rings	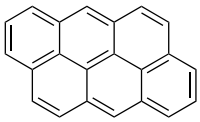
S_L (R)	1230	Aryl-alkyl ether	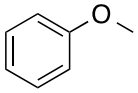
S	1185	C-C bonds between alkyl and aryl structures	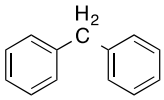
S_R (R)	1060	Substituted benzene ring	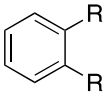

(R) denotes residual peak fits.

Li et al. [9] fit the bands from an amorphous, brown-coal carbon Raman spectrum to 9 distinct molecular structures (labeled G, G_R, V_R, V_L, D, S, S_R, and G_L) based on the vibrational spectroscopy literature. Figure SI-5 shows a representative Raman spectrum of HTC milled for 60 minutes, showing the raw data, the best-fit curves, and sum of the fit curves. The Li et al.[9] assignments provide a visibly good fit to the available data, with adjustments made only to the band intensities and widths, but not the peak locations.

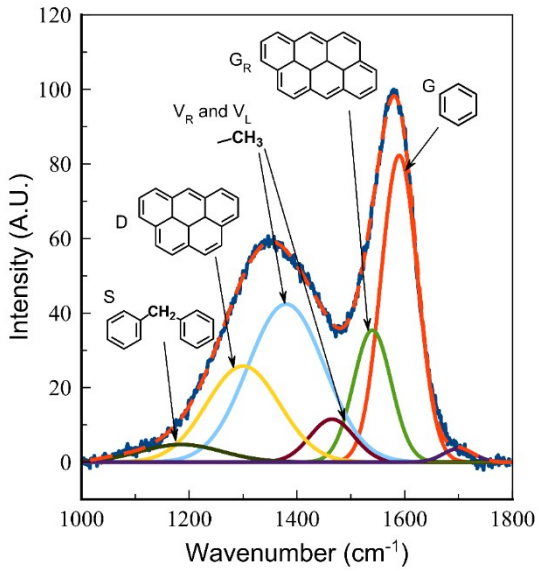

Figure SI-5. Peak fitting of Raman spectrum of a HTC ball-milled for 60 minutes using the assignments recommended by Li et al.[9] Peaks described in Table SI-1 are labeled, with the exception of residual peaks for G_L, S_L, S_R.

Tracking the relative ratios of these bands provides a method for following the molecular changes that occur during HTC milling. Following the recommendation of Li et al.,[9] we calculated the ratio of the S/G, $D/(G_R+V_L+V_R)$ and D/G_R from spectra obtained at each milling time. The S/G ratio reflects the relative intensity of bridge-head carbons compared to aromatic breathing modes; the $D/(G_R+V_L+V_R)$ ratio is related to the relative concentration of larger aromatic

structures containing more than 6 rings to several common defects; and the D/G_R ratio is related to the relative contributions of larger aromatic structures containing 6 or more rings to smaller aromatic structures containing 5 or fewer rings. The band intensity ratios were plotted against milling time as shown in Figure SI-6 shows a decrease in the S/G_R ratio with ball-milling time, indicating a decrease in alkyl branches in general, and specifically in bridge-head carbons, over time. Likewise, the D/G_R ratio increases over time, consistent with a relative increase of larger aromatic structures compared to smaller ones.

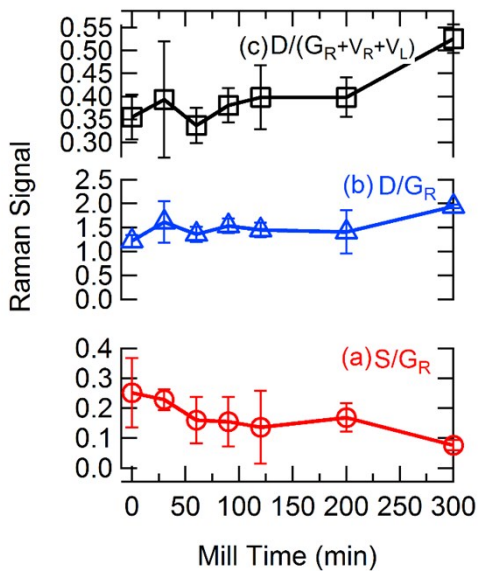

Figure SI-6. Raman peak fit ratios: bottom S/G_R; middle D/G_R; top $D/(G_R+V_L+V_R)$.

The observed S/G and D/G_R ratios suggest that ball milling breaks bridge-head carbon bonds (which are among the weakest carbon-carbon bonds present in the material based on binding energies[11]) with a subsequent shift from smaller aromatic structures to larger ones. Further evidence is provided by a deeper analysis of the Raman spectra. Previous studies have shown that structures with less than 6 aromatic rings in a chain do not influence the D band, but instead are seen in the G_R band at 1640 cm^{-1}.[9] These smaller aromatic structures are typically present in

amorphous carbon along with methyl and methylene groups (V_L and V_R bands) that join different aromatic ring chains into clusters. Li et al.[9] and other studies[12] have used the ratio $D/(G_R+V_L+V_R)$ as a measure of the concentration of small, highly amorphous short chain clusters relative to those contained in more structured 6+ aromatic ring structures shown by the D band. Figure SI-6 shows that the $D/(G_R+V_L+V_R)$ ratio has noticeably increased after 5 hours of ball-milling, indicating an increase in the amount of larger, 6+ aromatic ring structures in the sample relative to the small, amorphous clusters.

The transition between more amorphous short aromatic chains into larger, more locally organized >6 ring chains can be more clearly observed by comparing the D and G_R ratios. The transient response of $D/(G_R+V_L+V_R)$ ratio in Figure SI-6 a suggests that the D/G_R ratio should also increase with milling time. Figure SI-6c shows that indeed the D/G_R ratio increases with milling time, consistent with the hypothesis that ball milling gradually results in formation of more highly ordered aromatic domains over time. The gradual increase in aromatic order that we observe during ball milling is broadly consistent with the study of carbon heat treating reported by Bernarda et al.[8] Specifically, Bernarda et al.[8] used Raman and C-XANES spectroscopies to show that increasing heat treatment temperatures (up to >1000 °C) of a saccharose-based char material resulted in formation of localized, highly planar aromatic sub-domains within an otherwise amorphous structure. In our work, the intense, localized temperatures associated with ball milling impacts seem to be playing a similar role to the general thermal treatments used by Bernarda et al.[8]

To summarize, the Sadezky et al.[4] fitting scheme presented in the main text indicates that the HTC becomes more highly graphitic during ball milling and that a major contribution is the sequential formation and loss of graphene edges accompanied by an increase in graphene sheets.

The Li et al. [9] fitting scheme adds to this description by suggesting that primarily the weak bonds of aliphatic side chains and bridgehead carbon-carbon bonds break during ball milling, and that aromatic clusters consisting of <5 rings disappear with ball milling to be replaced by aromatic structures consisting of >6 rings. In sum, the main elements of the two fitting procedures[4, 9] are broadly consistent with one another; the Li et al. [9] fitting provides additional molecular level detail, at a significant expense of robustness as indicated by the substantially larger error bars shown in Figure SI-5 compared to those in Figure 6 in the text. Reconciling the molecular detail with a more robust fitting procedure is an active area of research in our group.

5. ESR Lineshape Analysis

ESR line shapes were fit using the Bruker Simfonia software assuming a single isotropic signal. A representative fit is shown in Figure SI-7 showing a much closer fit to a Lorentzian line shape than to a Gaussian line shape. Although the spectra all have nearly isotropic lineshapes that are best described as primarily Lorentzian, the lineshape did change with milling time. Specifically, spectra of unmilled HTC had a lineshape midway between Gaussian and Lorentzian while spectra of HTC milled for 120 minutes or longer had a more closely Lorentzian lineshape. HTC milled for less than 120 minutes had less symmetric spectra, which could be approximately simulated by a Lorentzian line with an anisotropic linewidth. The lack of resolution of the spectra means that a quantitative line shape analysis is not possible, but the evolution of the linewidth with increasing milling time indicates differences in the radical species that are present, with a significant change occurring after about 90 minutes of milling. High frequency (W-band) ESR analysis might be able to resolve these changes.[13]

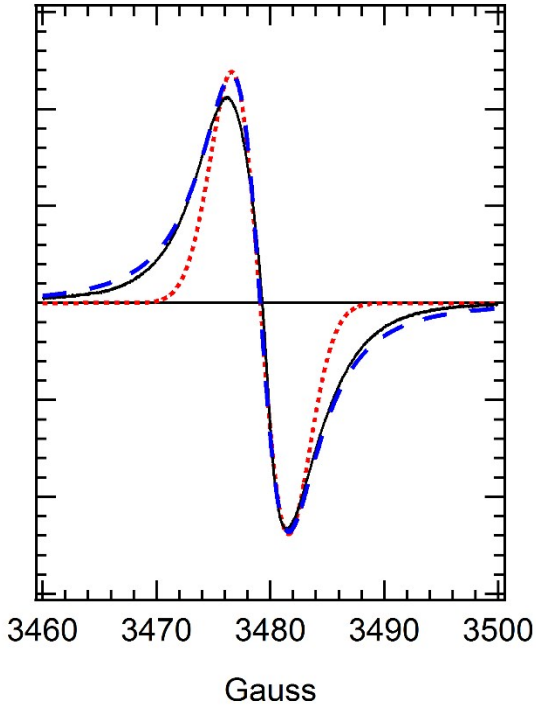

Figure SI-7. Example of ESR lineshape simulation; solid line (black): experimental spectrum for HTC milled for 30 min; dotted line (red): Gaussian lineshape fit with a 5G linewidth; dashed line (blue): Lorentzian lineshape fit with a 5G linewidth.

Cryogenic ESR measurements failed to improve resolution and in fact led to an increase in peak-to-peak linewidth (for example of a 90-min milled sample from 5.8G at 295K to 7.1G at 140K; increasing the temperature to 315K decreased the linewidth to 4.7G). These changes suggest that that there are temperature-dependent changes in the mobility of at least some of the radicals rather than in relaxation rates (which would lead to decreased linewidths at lower temperatures), and we propose that at low temperature the signals become more anisotropic and broader due to loss of averaging of the g and nuclear hyperfine tensors.[14, 15]

6. Influence of Bound Oxygen on ESR Spectra of HTC

ESR is sensitive to the presence of radicals. Oxygen, having two unpaired electrons, gives rise to broad ESR absorbance but at a magnetic field near 10,000 G at X-band, well-separated from the narrow g~2 signals observed for carbon-centered radicals.[16] Thus oxygen does not contribute to the observed EPR signals. However, oxygen can react with organic radicals reducing their concentrations. For this reason, we obtained ESR spectra of representative HTC samples both under air atmosphere and under vacuum to eliminate the effects of oxygen on the formation and decay of the observed radicals.[17] Samples stored under vacuum immediately after milling showed no statistically significant change in ESR signal intensity in the short term and no change in spectral resolution or g value. This indicates that oxygen does not cause line broadening or a significant amount of radical recombination after the sample is milled. We therefore conclude that the ESR data presented in the main text are not artificially inflated due to the adsorption of oxygen to the milled HTC surfaces. An *in situ* ESR measurement was beyond the scope of the present study and we did not attempt to mill under an oxygen-free environment (e.g., in a vessel filled with N_2 or Ar gas instead of air).

7. Supplemental SEM Micrographs

Figure 1 in the main text provides representative SEM micrographs for synthesized and milled HTC. Figures SI-8 through SI-12 provide additional SEM micrographs to support the statement in the main text that milling first induces HTC microsphere agglomeration and – at slightly longer time scales – conversion of spherical HTC particles into plate-like particles.

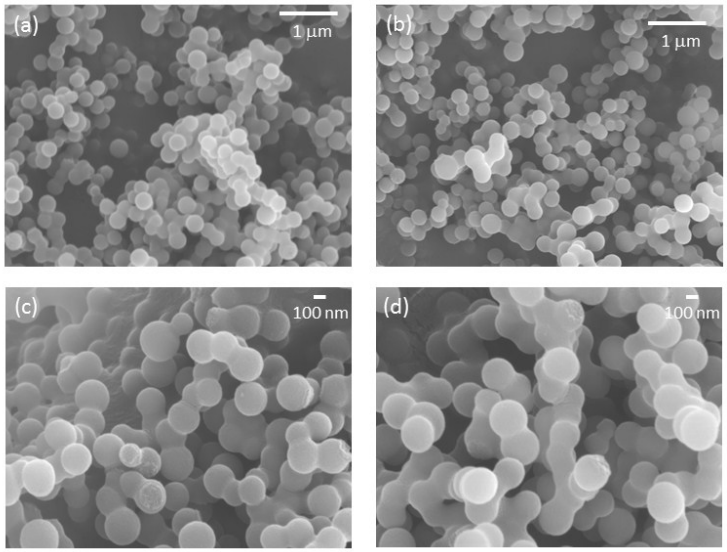

Figure SI-8. SEM micrographs obtained for synthesized HTC. Scale bars provided in figure.

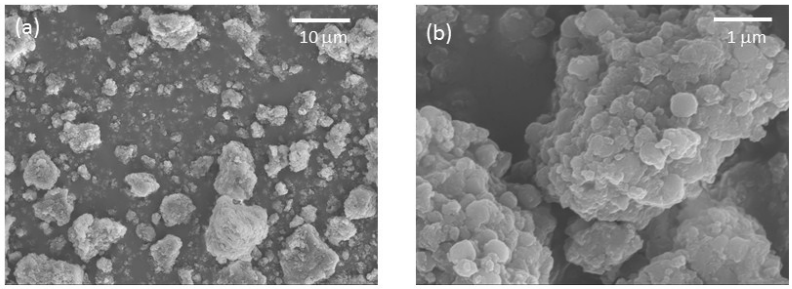

Figure SI-9. SEM micrographs obtained for HTC milled for 30 min. Scale bars provided in figure.

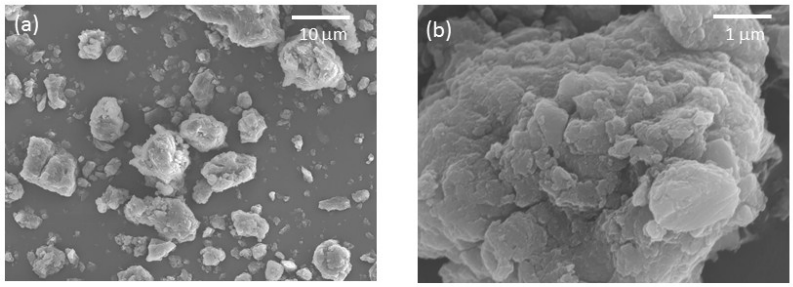

Figure SI-10. SEM micrographs obtained for HTC milled for 60 min. Scale bars provided in figure.

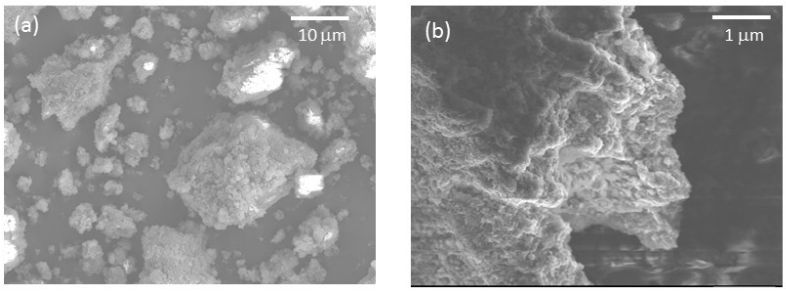

Figure SI-11. SEM micrographs obtained for HTC milled for 90 min. Scale bars provided in figure.

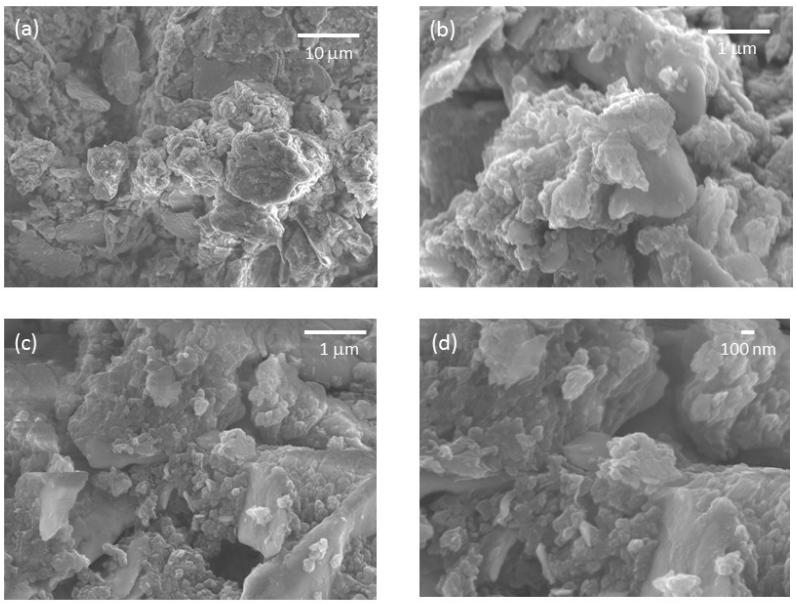

Figure SI-12. SEM micrographs obtained for HTC milled for 200 min. Scale bars provided in figure.

7. Characteristic Bond Energies in HTC

In the text, we present bond energy data for several characteristic bonds thought to be present in HTC. In Table SI-2, we provide a more thorough summary of bond energy data.

Bond	Energy (kJ/mol)	Source
C-C	347	Carruth and Ehrlich[18]
C-O	358	Carruth and Ehrlich [18]
(C)Ar-(C)Ar biphenyl	372.5	Fliszar[19]
(C)Ar-H benzene	466	Fliszar[19]
C6H5-OH	463.6	Handbook of Chemistry and Physics[20]
C6H5-OCH3	418.8	Handbook of Chemistry and Physics[20]
C6H5-CH3	426.8	Handbook of Chemistry and Physics[20]
C6H5-H	465.9	Handbook of Chemistry and Physics[20]
C6H5-COOH	429.7	Handbook of Chemistry and Physics[20]
C6H5-OC6H5	326.8	Handbook of Chemistry and Physics[20]
C6H5-C6H5	478.6	Handbook of Chemistry and Physics[20]
C6H5-COCH3	406.7	Handbook of Chemistry and Physics[20]

References

1. C. Russo, F. Stanzione, A. Tregrossi and A. Ciajolo, *Carbon*, 2014, **74**, 127-138.
2. R. Sanderson, *Chemical Bonds and Bonds Energy*, Elsevier, 2012.
3. V. S. Babu and M. Seehra, *Carbon*, 1996, **34**, 1259-1265.
4. A. Sadezky, H. Muckenhuber, H. Grothe, R. Niessner and U. Pöschl, *Carbon*, 2005, **43**, 1731-1742.
5. O. Beyssac, B. Goffe, J. P. Petitet, E. Froigneux, M. Moreau and J. N. Rouzaud, *Spectrochimica Acta Part A: Molecular and Biomolecular Spectroscopy*, 2003, **59**, 2267-2276.

6. C. Beny-Bassez and J. Rouzaud, *Scanning Electron Microscopy*, 1985, **1**, 119-132.

7. G. S. Foo and C. Sievers, *ChemSusChem*, 2015, **8**, 534-543.

8. S. Bernarda, O. Beyssac, K. Benzerara, N. Findling, G. Tzvetkov and G. E. Brown Jr., *Carbon*, 2010, **48**, 2506–2516.

9. X. Li, J.-I. Hayashi and C.-Z. Li, *Fuel*, 2006, **85**, 1700-1707.

10. M. Sevilla and A. B. Fuertes, *Chemistry - A European Journal*, 2009, **15**, 4195-4203.

11. *CRC Handbook of Chemistry and Physics, 92nd Edition*, CRC, 2011.

12. M. Asadullah, S. Zhang, Z. Min, P. Yimsiri and C.-Z. Li, *Bioresource Technology*, 2010, **101**, 7935-7943.

13. R. Clarkson, W. Wang, D. Brown, H. Crookham and R. Belford, *Advances in Chemistry Series*, 1993, **229**, 507-507.

14. A. Gutsze and S. Orzeszko, *Advances in Colloid and Interface Science*, 1985, **23**, 215-233.

15. R. Barklie, M. Collins and S. Silva, *Physical Review B*, 2000, **61**, 3546.

16. B. Ranby and J. F. Rabek, *ESR spectroscopy in polymer research*, Springer Science & Business Media, 2012.

17. A. Manivannan, M. Chirila, N.C. Giles and M. S. Seehra, *Carbon*, 1999, **37**, 1741–1747.

18. G. Carruth and E. Ehrlich, *Bond Energies*, Southwestern, Tennessee, 2002.

19. S. Fliszár, Springer, 1994.

20. *Journal*, 2015.